The effect of failure criteria on risk-based inspection planning of offshore wind support structures

Nandar Hlaing, Pablo G. Morato & Philippe Rigo
Naval & Offshore Engineering, ArGEnCo, University of Liege, 4000 Liege, Belgium

Peyman Amirafshari & Athanasios Kolios
Department of Naval Architecture, University of Strathclyde, Glasgow G4 0LZ, United Kingdom

Jannie S. Nielsen
Department of the Built Environment, Aalborg University, 9220 Aalborg, Denmark

ABSTRACT: Offshore Wind Turbine (OWT) support structures are subjected to harsh deterioration mechanisms due to the combined action of wind loading, sea induced load actions and corrosive environment. Fatigue failure becomes a key failure mode for offshore wind structures, as they experience considerable number of stress cycles (more than 10 million cycles per year). Fatigue failure can be assessed through fatigue assessment approaches. However, such assessments possess various uncertainties which may be quantified and updated through findings from in-service inspections. Since, offshore maintenance actions incur significant costs, an optimal maintenance strategy which balances the maintenance efforts against the risk of failure is desired. Based on pre-posterior decision theory, a risk-informed maintenance optimization can be performed to define the optimal maintenance strategy and support the decision maker(s). Within the risk maintenance optimization scheme, the probabilistic deterioration model is updated based on the inspection outcomes. Several fracture mechanics models have been used in the literature to estimate the deterioration of the structure containing flaws. Although, a through-thickness failure criterion is commonly used in the literature as the failure criteria, a Failure Assessment Diagram (FAD) approach has been receiving increasingly attention, as well. This investigation examines the effect of the selected fracture mechanics models and failure criteria on the optimal maintenance strategy. Moreover, the obtained maintenance strategies corresponding to different fracture mechanics models are compared for a tubular joint case study structure.

1 INTRODUCTION

For offshore wind structures, it is important to minimize Levelized Cost of Energy (LCOE). LCOE is the ratio of the present values of total expected cost of a wind turbine over the energy production in its lifetime. Identifying optimal maintenance strategies has been demanded to balance between the failure probability and maintenance efforts leading to minimize total expected cost.

In risk-based inspection planning, conventional through-thickness failure criterion is conservative for some redundant structures like jacket type OWTs. These structures have the capacity to sustain through-thickness cracks until the loading exceeds the resistance of the cracked structure. Thus, the use of Failure Assessment Diagram (FAD) as a limit state function is introduced. Radu & Sedmak (2016) performed reliability assessment of welded joints by fracture me-

chanics approach where the failure is defined by a FAD. Similar work was done by Chocat, Beaucaire, Debeugny, Lefebvre, Sainvitu, Breitkopf, & Wyart (2016) but the reliability was computed by using First Order Reliability Method (FORM) with a Surrogate-based Optimization (SBO) algorithm. Mai, Sørensen, & Rigo (2016) performed the reliability updating of a tubular welded joint in offshore wind structures using FAD as failure criterion in the limit state function.

This paper explores the influence of fracture mechanics models and failure functions on optimal inspection planning. A simplified framework of risk-based inspection planning is presented. Failure probabilities from fatigue SN model are used as reference data and different fracture mechanics models are calibrated to the SN model so that the inspection outcomes can be incorporated. Two different fracture mechanics approaches have been used to describe
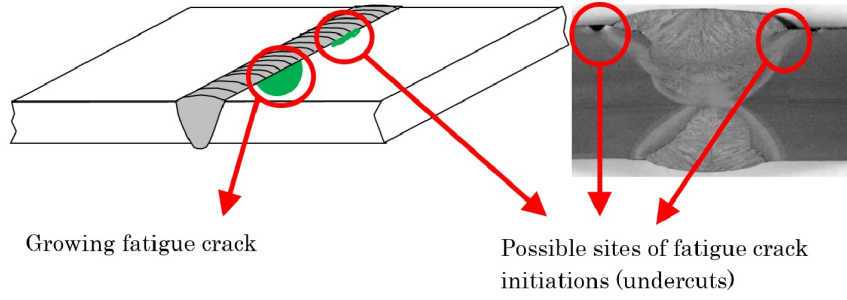
Figure 1: Illustration of fatigue crack initiation

the crack propagation. Two-dimensional crack growth models are more complex and precise with inclusion of the effects due to time-dependent crack size, geometry of the structure and welded detail. The main limitation of 2-D FM models is that they require large computational time, about 500 times that of 1-D models. The risk-based inspection framework is applied to the case of a tubular joint to define optimal inspection planning for each combination of FM model and failure criterion. Finally, optimal intervals of inspection and optimal annual failure probability thresholds are compared for different FM models and failure criteria. The effect of failure criteria on the optimal inspection plan is examined.

2 FAILURE CRITERIA

Fatigue cracks in welded structures initiate from weld fabrication imperfections at the joints as illustrated in Figure 1. The initiated crack grows both through the thickness of the plate and along the weld line until the failure occurs. Assuming that the thickness is smaller than the length and the width of the member, the crack is likely to penetrate the whole thickness first. The failure criteria depend on the ability of the structure to further resist the applied load after through-thickness penetration.

2.1 *Through-thickness Failure Criterion*

In the through-thickness criterion, the initial fatigue crack is assumed to be a surface breaking flaw growing along the height and length of the flaw. The failure happens when the crack height reaches the thickness of the structure which is also the critical crack size a_{crit}. This common criterion is particularly adopted for structures containing pressurised containment e.g. pipe lines, pressure vessels, etc.

$$g_{FM}(t) = a_{crit} - a(t) \tag{1}$$

2.2 *Failure Assessment Diagram*

When a crack propagates through a structure, ultimately the crack size reaches a critical size which corresponds to a critical stress intensity factor, usually taken as the characteristic value of the fracture

toughness K_{mat}, at which fracture happens. Alternatively, if the applied load is high and the structure tensile strength is low, the structure may reach its tensile capacity and fails by plastic collapse. The failure assessment diagram combines these two failure modes. In between brittle fracture and plastic collapse is an elastoplastic failure mode, where the failure occurs before reaching the plastic capacity or toughness (Amirafshari 2019).

The failure assessment line (FAL) represents the critical values of crack driving parameter:

$$K_{r,crit} = \frac{K_{elastic}}{K_{elastoplastic}} \tag{2}$$

$K_{r,crit}$ is equal to 1 when the applied load is zero and declines as the ratio between applied load and yield load L_r increases towards the collapse load as in Figure 2. BS7910 (2015) provides three alternative options to determine the FAL. These are of increasing complexity in terms of the required material and stress analysis data but provide results of increasing accuracy. Examples of failure assessment diagrams are shown in Figure 2. If the assessment point lies inside the envelope below the assessment line, the fracture mechanics driving parameter is lower than the materials resistance parameter and the part should be safe, otherwise there is a failure. As it is illustrated, FAD can be categorised into three different zones: Zone I is the fracture dominant zone, Zone II is the elastoplastic zone and Zone III is the plastic collapse dominant zone.

When FAD is used as limit state function, the failure occurs when the stress exceeds the reduced capacity of the cracked structure. It becomes necessary to consider the combined influence of applied loads and non-monotonic strength deterioration of the cracked structure. Thus, to evaluate the failure probability with FAD requires to apply time-variant reliability methods which are extremely time-consuming. Time-variant reliability analysis is still an ongoing research field and will not be studied in this work.

A simplified and conservative criterion proposed by JCSS (2011) has been used in this work as alternative to FAD. The failure is expected if the interaction of crack-driving parameter K_r and the ratio between applied load and yield load L_r exceeds a normalised resistance parameter R_f, with the mean value as plotted
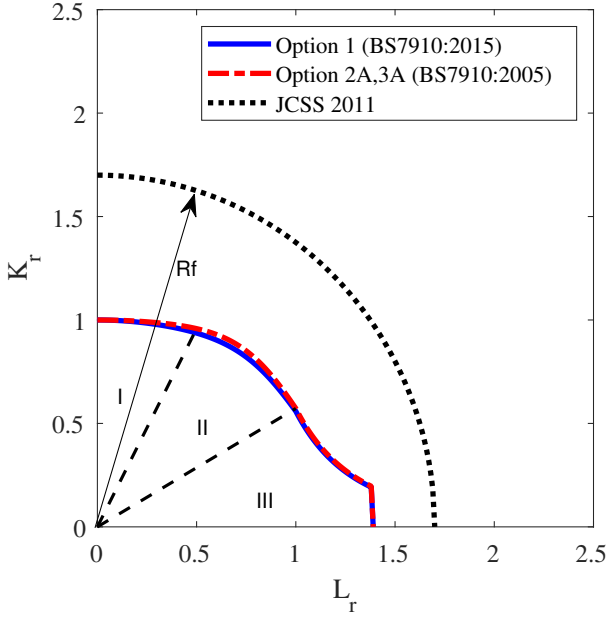
Figure 2: Failure assessment diagrams

in Figure 2. Then, limit state equations and assessment points are reformulated as

$$g_{FM}(t) = R_f - \sqrt{K_r^2(t) + L_r^2(t)} \qquad (3)$$

$$K_r = \frac{K_I}{K_{mat}} + \rho \qquad (4)$$

$$L_r = \frac{\sigma_{ref}}{\sigma_Y} \qquad (5)$$

where R_f is the normalised resistance parameter (JCSS 2011). K_I is the stress intensity factor calculated at the crack tip. K_{mat} is the fracture toughness of the material. σ_{ref} is the net section stress or reference stress of the cracked structure and σ_Y is the yield stress. The plasticity correction factor ρ represents the reduced load carrying capacity of the deteriorated structure and increases as the crack size becomes larger. The plasticity correction can be evaluated according to the procedures in JCSS (2011).

3 RISK-BASED INSPECTION PLANNING METHODOLOGY

This section presents the procedures to create a risk-based inspection model aiming to define the optimal inspection policy. The RBI model is based on the probabilistic fatigue approach. Different combinations of fracture mechanics models and failure criteria are implemented to examine their effects on the optimal inspection plan.

3.1 *Fatigue Modelling*

Offshore wind turbine support structures are subjected to a large number of load cycles in their lifetime. For such structures, the long-term stress range distribution can be efficiently represented by a two-parameter Weibull distribution, described by a scale

parameter q and a shape parameter h. The shape parameter h is taken as 0.8 (DNVGL-RP-C210 2019) and the scale parameter q is computed from Eq. (6).

$$D = nT_d \left[\frac{q^{m_1}}{a_1} \Gamma \left(1 + \frac{m_1}{h}; \left(\frac{S_1}{q} \right)^h \right) \right.$$

$$\left. + \frac{q^{m_2}}{a_2} \gamma \left(1 + \frac{m_2}{h}; \left(\frac{S_1}{q} \right)^h \right) \right] \qquad (6)$$

where D is the accumulated fatigue damage considered for the selected Fatigue Design Factor FDF and design life T_d. m_1, m_2, a_1, a_2, S_1 are parameters of the bi-linear SN curve. n is the number of stress cycles per year. Γ and γ are incomplete gamma functions.

3.2 *Crack Growth Modelling*

Imperfections in the welding process of offshore wind support structures can be considered as initial cracks and they grow under cyclic loading in the harsh environment. Paris-Erdogan's law has been widely used in Linear Elastic Fracture Mechanics (LEFM) to model the crack growth as in Eq. (7) and Eq. (8):

$$\frac{da}{dn} = C_a(\Delta K_a)^m \qquad (7)$$

$$\frac{dc}{dn} = C_c(\Delta K_c)^m \qquad (8)$$

where a and c are the crack depth and crack length respectively, n is the number of stress cycles, C_a, C_c and m are Paris law parameters, also called crack growth parameters. ΔK is the stress intensity factor range at the crack tip calculated for the applied stress range as in Eq. (9) and Eq. (10).

$$\Delta K_a = \Delta \sigma Y_a(a,c) \sqrt{\pi a} \qquad (9)$$

$$\Delta K_c = \Delta \sigma Y_c(a,c) \sqrt{\pi a} \qquad (10)$$

where Y_a and Y_c are stress intensity correction factors or geometry factors and are dependent on the geometry of the component, welded joint detail and two-dimensional crack size.

3.2.1 *One-dimensional crack growth model*
Crack propagation in the direction of crack depth is described by the following differential equation:

$$\frac{da}{dn} = C_a \left[\Delta \sigma Y_a(a) \sqrt{\pi a} \right]^m \qquad (11)$$

Considering one-dimensional crack model, the stress intensity correction factor Y_a simply becomes a function of crack depth only. If it is assumed that the geometry factor Y_a does not depend on the time-varying

crack depth and it is approximated as a constant value over the lifetime, an explicit solution of the crack growth can be obtained as in Eq. (12) (Ditlevsen & Madsen 2007).

$$a(t) = \left[\left(1 - \frac{m}{2}\right) C_a Y_a^m \pi^{m/2} (\Delta\sigma)^m n \right.$$

$$\left. + a_{t-1}^{1-m/2} \right]^{(1-m/2)^{-1}} \quad (12)$$

3.2.2 *Two-dimensional crack growth model*

At each time step, the evaluation of the second dimension, crack length c is accompanied with that of crack depth a. Since both Y_a and Y_c have dependencies on a and c, a pair of coupled differential equations, Eq. (7) and Eq. (8), is to be simultaneously solved.

The stress range distribution is assumed to be composed of membrane and bending stresses. The two components are quantified by the ratio of bending stress to total stress, called the degree of bending DOB. Stress concentration due to weld geometry is incorporated as the stress magnification factor M_k. The stress intensity factor ranges finally become as in Eq. (13) and Eq. (14).

$$\Delta K_a = \Delta\sigma \Big[Y_{ma} M_{kma} (1 - DOB)$$

$$+ Y_{ba} M_{kba}\, DOB \Big] \sqrt{\pi a} \quad (13)$$

$$\Delta K_c = \Delta\sigma \Big[Y_{mc} M_{kmc} (1 - DOB)$$

$$+ Y_{bc} M_{kbc}\, DOB \Big] \sqrt{\pi a} \quad (14)$$

The subscripts a, c mean crack depth and length and m, b refer to membrane and bending stress components. Geometry functions $Y_{ma}, Y_{ba}, Y_{mc}, Y_{bc}$ and stress magnification factors $M_{kma}, M_{kba}, M_{kmc}, M_{kbc}$ can be solved by finite element methods or by means of parametric equations, for instance, as in BS7910 (2015).

3.3 *Calibration of FM Model to SN Model*

Since the design of offshore substructures are based on fatigue model and inspection planning demands for the crack growth, FM models are calibrated to the SN model. Initial crack size and crack growth parameters are calibrated for each FM model so that the reliability according to SN and FM approaches are similar over the lifetime. Calibration is performed by the least-square fitting of the normalized failure probability.
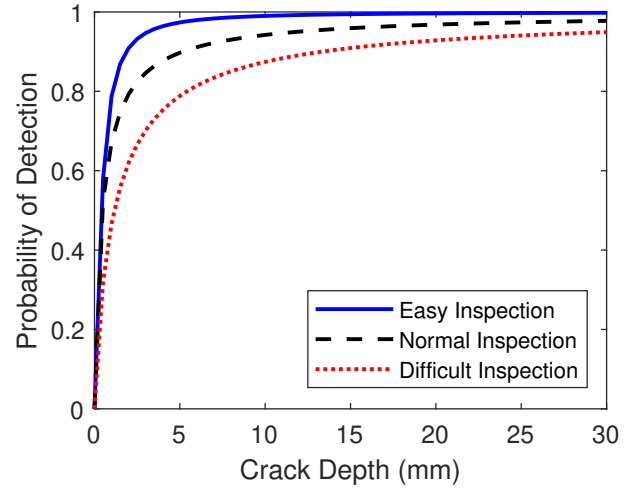

Figure 3: PoD curves for EC inspection

3.4 *Inspection Modelling*

Uncertainties in the inspection are considered by modelling the probability of detection (PoD). PoD curves for different inspection methods are provided in DNVGL-RP-C210 (2019). Eddy Current inspection (EC) has become a preferred inspection method for offshore structures as it can be used to detect fatigue cracks without removing coating. The distribution function of PoD curves can be represented as

$$PoD(a_d) = 1 - \frac{1}{1 + \left(\frac{a_d}{X_0}\right)^b} \quad (15)$$

where a_d is the detectable crack depth, X_0 and b are the distribution parameters dependent on the method and conditions of inspection. PoD curves for EC inspection for different working conditions according to DNVGL-RP-C210 (2019) are shown in Figure 3. The failure probability after the inspection can be computed using event updating. For instance, under the condition of no crack detected during inspection, the updated failure probability is:

$$P_F(t) = P(a(t) > a_{crit} \mid a_{ins} < a_d)$$

$$= \frac{P(a(t) > a_{crit} \cap a_{ins} < a_d)}{P(a_{ins} < a_d)} \quad (16)$$

where a_{crit} is the critical crack size and a_{ins} is the crack size at the time of inspection.

3.5 *Cost Modelling and Optimization*

The objective of maintenance optimization is to minimize the total expected cost which includes failure cost, inspection cost and repair cost. The expected cost of each inspection plan C_{total} is computed as described in Eq. (17) from the cost models C_F, C_I, C_R and the probabilities P_F, P_R. A proper value of discount rate r is applied to account for time value of

money (Straub 2004).

$$C_{total} = C_F \left[\frac{P_{F,t=1}}{1+r} + \sum_{t=2}^{T_{SL}} \frac{\Delta P_{F,t}(1-P_{F,t-1})}{(1+r)^t} \right] + C_R$$

$$\sum_{t=t_{Ins,1}}^{T_{Ins,N}} \frac{P_{R,t}(1-P_{F,t})}{(1+r)^t} + C_I \sum_{t=t_{Ins,1}}^{T_{Ins,N}} \frac{(1-P_{F,t})}{(1+r)^t} \quad (17)$$

T_{SL} is the lifetime of the structure. $\Delta P_{F,t}$ is the annual probability of failure in year t, given no failure before year t. The probability of repair at year t, $P_{R,t}$, is computed in such a way that crack detected during inspection is repaired and after repair, it behaves like being not detected.

It is theoretically feasible to obtain optimal inspection plan by means of the pre-posterior decision theory, however it requires great computational efforts (Straub 2004). To simplify this problem, two heuristic approaches have been proposed by Faber (2000). These are periodic interval approach and constant threshold approach from which optimal interval and optimal annual failure probability threshold can be identified.

4 APPLICATION TO A TUBULAR JOINT

4.1 Fatigue Modelling

The RBI framework presented in the previous section is applied to the case of a tubular joint. From DNVGL-ST-0126 (2018), considering the case of upper splash zone above mean waterline accessible for inspection, Fatigue Design Factor FDF can be taken as 2 and the damage $D = 0.5$ is used to calibrate the scale parameter q for the Weibull stress range distribution. In this paper, bi-linear SN curve for tubular joints in air environment is used (DNVGL-RP-C203 2016). From Eq. (6), the scale parameter $q = 6.4839$ is obtained to accumulate a fatigue damage of $D = 0.5$ for a design life of 20 years. The variables used in the SN approach are described in Table 1.

Reliability over the lifetime according to the SN Miner's Rule is computed by Monte Carlo simulations with one million samples. Figure 4 shows the expected value of the cumulative failure probability and 95 percent confidence interval.

4.2 Parameters of FM Models

4.2.1 Incorporation of residual stress

For the case of welded joints, it is necessary to take account of residual stress as a consequence of weld metal contraction being restrained by the base material (Anderson 2005). The presence of uniform residual stress in welded joints contributes as secondary stress component in the stress intensity factor as $K_I =$

Table 1: Variables used in SN approach

Variable	Distrib.	Mean (Median)	Std (CoV)
m_1	Determ.	3	
m_2	Determ.	5	
$log_{10}(a_1)$	Normal	12.48	0.2
$log_{10}(a_2)$	Normal	16.13	0.2
S_1	Determ.	67.09	
n	Determ.	$3.5 \cdot 10^7$	
q	Normal	6.4839	0.2
h	Determ.	0.8	
Δ	LN	(1)	(0.3)

Determ. = Deterministic, LN = Lognormal
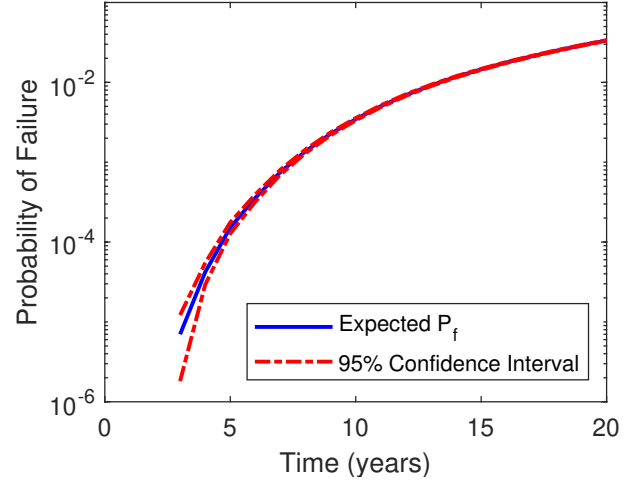*$log_{10}(a_1)$ and $log_{10}(a_2)$ are fully correlated.

Figure 4: Cumulative failure probability with fatigue SN Model

$K_I^P + K_I^S$. However, secondary stress does not contribute in the plastic collapse since it has no significant effect on the tensile strength (BS7910 2015). Realistic estimates of residual stress are possible by finite element simulations of welding. For the case of unavailable FEM solutions, residual stress can be assumed to be uniform which is conservative (JCSS 2011).

4.2.2 Tensile strength and fracture toughness

Material properties are considered as uncertainties due to production variability. Distribution of tensile strength is often assumed to follow a lognormal distribution. Fracture toughness is a quantitative description of material's resistance to fracture failure beyond which the crack propagation becomes unstable and unlimited. Three-parameter Weibull distribution is proposed to describe the fracture toughness K_{mat} as in Eq. (18) (JCSS 2011).

$$F_{Kmat}(k) = 1 - exp \left[- \left(\frac{k - K_0}{A_k} \right)^{B_k} \right] \quad (18)$$

The shape parameter B_k is taken as 4 and the recommended value of the threshold parameter K_0 is 20 MPa$\sqrt{m}$ (JCSS 2011). The scale parameter A_k is computed as in Eq. (19) (BS7910 2015). The resulting

fracture toughness is in MPa$\sqrt{m}$.

$$A_k = \left[11 + 77 \, exp \left(\frac{T - T_0 - T_K}{52} \right) \right]$$

$$\left(\frac{25}{B} \right)^{0.25} \left[ln \left(\frac{1}{1-p} \right) \right]^{0.25} \quad (19)$$

where T is the temperature at which K_{mat} is to be determined (in °C). T_0 is the temperature for a median toughness of 100 MPa$\sqrt{m}$ in 25 mm thick specimens and calculated as $T_0 = T_{27J} - 18°C$. T_{27J} is the temperature for $27J$ measured in a standard Charpy V specimen. T_K is the temperature term that describes the scatter in the Charpy versus fracture toughness correlation. For $Std = 15°C$ and 90 percent confidence, T_K is +25°C. B is the thickness of the material for which an estimate of K_{mat} is required (in mm). and p is the probability of K_{mat} being less than estimated and 5 percent is recommended without experimental evidence. The material is chosen to be $EN10025 - S355 - JR$ and the required values are obtained from Igwemezie, Mehmanparast, & Kolios (2018) as $T = 10$ °C, $T_{27J} = 20$ °C and $\sigma_Y = 355$ MPa.

4.3 SN-FM Calibration

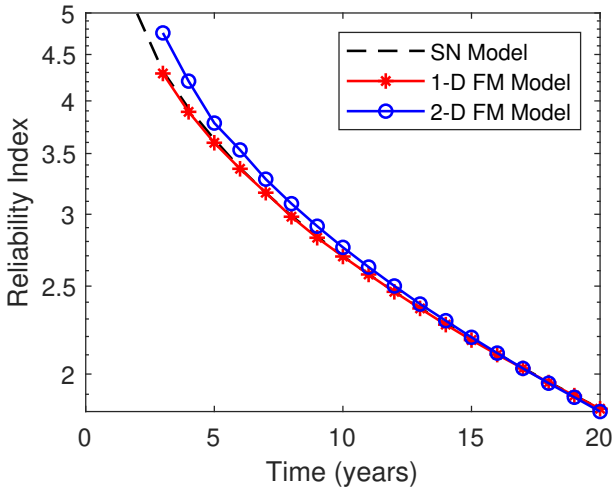

Figure 5: Calibration between SN and FM approaches

Three different combinations of FM models and limit states are studied in this paper.

Option 1: One-dimensional crack growth + Through-thickness failure criterion
Option 2: Two-dimensional crack growth + Through-thickness failure criterion
Option 3: Two-dimensional crack growth + Simplified FAD failure criterion

The initial crack size a_0 and crack growth parameter C_a are calibrated to get the same reliability

in SN and FM models. In option 3, through-thickness failure criterion is still used for the calibration due to the assumption that the cracks are failed when they penetrate the thickness during SN tests. The simplified FAD failure criterion is only used for inspection planning. Figure 5 shows the goodness-of-fit for the calibrations. The calibration for the 2-D FM model is not perfect in high reliability region. But the probabilities of failures in this region are really small so that they are assumed not to affect the optimal decision. The calibrated parameters together with all other parameters used in FM models are listed in Table 2. The values of R_s and R_f used in option 3 are as recommended in JCSS (2011).

Table 2: Variables used in FM approach

Variable	Option	Distrib.	Mean (Median)	Std (CoV)
*a_0	1	Exp.	0.1235	
	2,3	Exp.	0.1603	
*$log(C_a)$	1	Normal	-27.7903	0.3473
	2,3	Normal	-27.6302	0.4599
n	1,2,3	Determ.	$3.5 \cdot 10^7$	
h	1,2,3	Determ.	0.8	
m	1,2,3	Determ.	3	
q	1,2,3	Normal	6.4839	0.2
a_{crit}	1,2	Determ.	16	
Y_a	1	LN	(1)	(0.1)
a_0/c_0	2,3	Determ.	0.2	
DOB	2,3	Determ.	0.81	
C_a/C_c	2,3	Determ.	1	
R_s	3	LN	(300)	(0.2)
σ_Y	3	LN	(355)	(0.07)
K_{mat}	3	3P-W		
R_f	3	LN	(1.7)	(0.18)

Determ. = Deterministic, Exp. = Exponential,
LN = Lognormal, 3P-W = Three-parameter Weibull
*Calibrated parameters

4.4 Crack Growth

This section describes the propagation of crack over the lifetime. As mentioned in the previous sections, both 1-D and 2-D crack growth models are applied to estimate the deterioration. In both models, the crack propagation rate is influenced by the Paris law parameters C_a and the geometry factor Y.

To represent one-dimensional crack growth, Ditlevsen's FM model is used where the geometry factor is independent of time-varying crack size and approximated as a uniform value over the lifetime.

In two-dimensional crack growth, the geometry factors Y_a and Y_c become functions of time-varying crack size and are recomputed at every time step. The geometry functions and magnification factors are evaluated by parametric equations following the procedures of Newman & Raju (1981) and DNVGL-RP-C210 (2019). The propagation of mean crack depth and crack length is illustrated in Figure 6. The crack grows faster in 2-D model than in 1-D model due to higher calibrated Paris law parameter C_a in the former option.
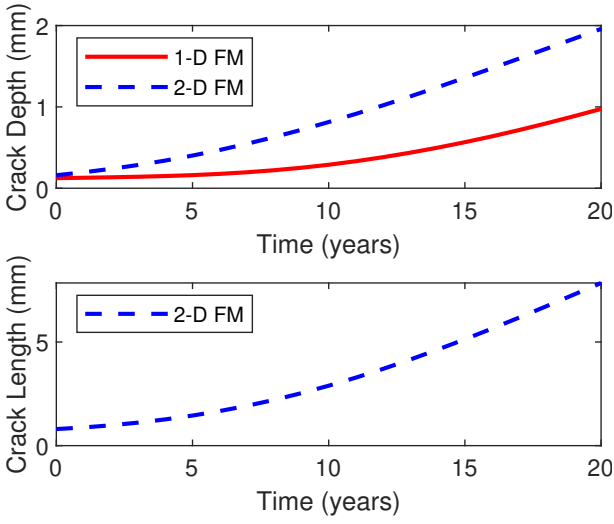
Figure 6: Illustration of mean crack propagation
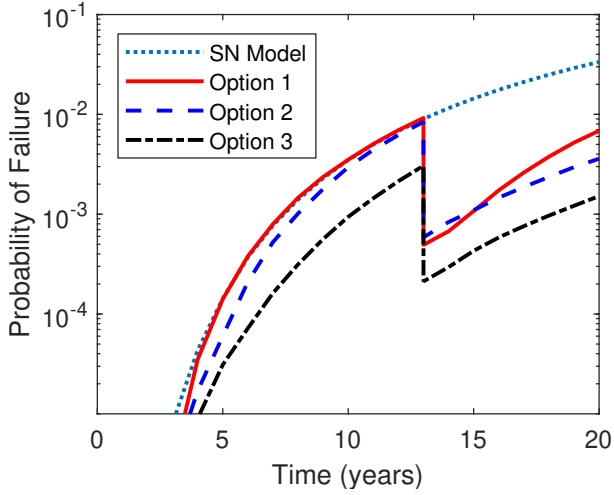
4.5 *Updating Reliability*

Figure 7: Updated failure probability after inspection

The effect of failure criteria on the updated failure probability after an inspection is examined. Assuming an inspection is performed at year 13 and no crack is detected during inspection, and the reliability is updated for different options. As shown in Figure 7, it can be seen that the updated failure probabilities are different for each case. Option 3 gives the smallest failure probabilities due to the assumption of capacity to hold the through-thickness cracks. When the 2-D crack growth model is used, the crack size at the year of inspection is larger and the probability of detection is increased. And contrarily, the updated probability of failure in option 2, given that no crack is detected, becomes smaller compared to option 1 according to Eq. (16).

4.6 *Optimal Maintenance Strategies: Results and Discussion*

Two heuristic models have been applied to generate the optimal maintenance policies (optimal interval and optimal failure threshold). The failure of the

tubular joint costs 10^6 monetary units. The cost of inspection is 10^3 monetary units and the repair expenses for 10^4 monetary units. A discount rate of 6 percent is incorporated. The risk-based inspection models associated with the total costs are plotted in Figure 8 and Figure 9.
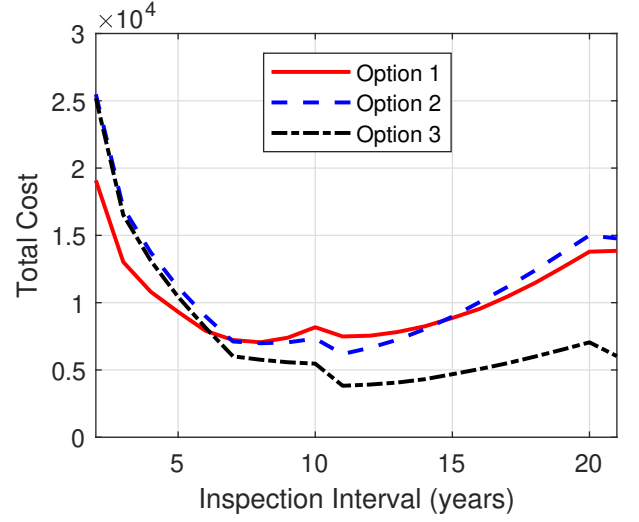

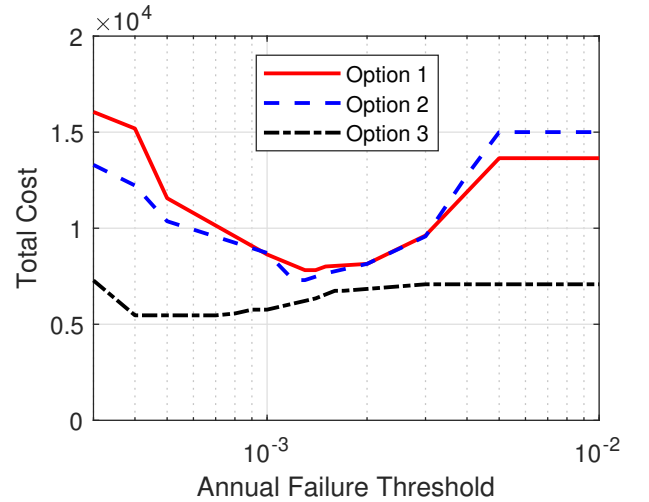Figure 8: Periodic interval risk-based inspection

Figure 9: Annual failure probability threshold risk-based inspection

Table 3 compares the optimal inspection plans and costs for each option with periodic interval approach. With option 1, the optimal interval is 8 years and two inspections have to be carried out during the lifetime. With options 2 and 3, the optimal plan is to inspect only once at year 11. Table 4 shows the optimal thresholds, as well as the years at which the inspections have to be performed and their respective costs. In option 1, two inspections have to be performed at year 10 and 16. One inspection has to be done at year 10 for option 2 and at year 11 for option 3.

Table 3: Optimal inspection intervals

	Optimal interval	$\sum C_F$ $(.10^3)$	$\sum C_I$ $(.10^3)$	$\sum C_R$ $(.10^3)$	C_{Total} $(.10^3)$
Option 1	8	3.354	1.021	2.682	7.057
Option 2	11	3.535	0.527	2.122	6.184
Option 3	11	1.177	0.527	2.131	3.825

Table 4: Optimal faiure thresholds

	Optimal threshold	$\sum C_F$ ($.10^3$)	$\sum C_I$ ($.10^3$)	$\sum C_R$ ($.10^3$)	C_{Total} ($.10^3$)
Option 1	0.0013 (10, 16)	2.992	1.263	3.5628	7.818
Option 2	0.0012 (10)	2.773	0.869	3.656	7.299
Option 3	0.0006 (11)	1.044	0.838	3.581	5.463

It can be noted that the last two options give less number of inspections in optimal RBI planning as well as lower total expected costs. Significant reduction of failure costs has been observed by the used of FAD as failure criterion as shown in Figure 10. The through-thickness cracks which are assumed as failed in Option 1 and 2 can grow further in length until the critical value of the stress intensity factor is reached. It is worth mentioning that the fracture toughness of the material considered for the tubular joint is high enough so that the component does not fail before the crack reaches the thickness and can hold the through-thickness crack. The 2-D FM model causing the rapid growth of crack compared to 1-D model significantly contributes to increase in the repair cost per inspection since PoD is higher for bigger cracks.
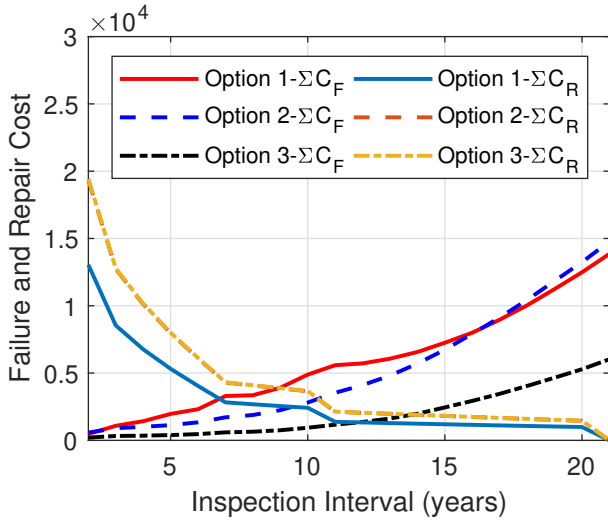

Figure 10: Comparison of failure and repair costs

5 CONCLUSION

In this paper, the effect of failure criteria on risk-based inspection planning of offshore wind structures is studied with the incorporation of different fracture mechanic models. The calibration of FM models to SN data offers a deterioration framework where inspection outcomes can be incorporated, keeping the empirical nature of SN model. The 2-D FM model is more detailed than 1-D model but it requires FEM solutions of the geometry factor. Alternatively, the use of parametric equations, as in this work, requires more computational time than 1-D model.

The effect of different failure criteria on the updated failure probability after an inspection is presented. Finally, it is proven that the choice of failure criteria and fracture mechanics model can affect the optimal inspection solution. For redundant structures with high fracture toughness, using FAD failure criteria gives less total expected cost. The decision maker(s) should keep it in mind and the appropriate failure criterion should be wisely chosen depending on the properties of the material used, the nature of the structure, and the loading condition.

ACKNOWLEDGEMENT

REFERENCES

Amirafshari, P. (2019). *Optimising non-destructive examination of newbuilding ship hull structures by developing a data-centric risk and reliability framework based on fracture mechanics*. Ph. D. thesis, University of Strathclyde, Glasgow.

Anderson, T. L. (2005, June). *Fracture mechanics: Fundamentals and applications*. Taylor and Francis Group.

BS7910 (2015). *Guides to methods for assessing the acceptability of flaws in metallic structures*. British Standards.

Chocat, R., P. Beaucaire, L. Debeugny, J.-P. Lefebvre, C. Sainvitu, P. Breitkopf, & E. Wyart (2016, 01). Reliability analysis in fracture mechanics according to combined failure criteria. In *Proceedings VII European Congress on Computational Methods in Applied Sciences and Engineering*, pp. 6721–6733.

Ditlevsen, O. & H. O. Madsen (2007). *Structural reliability methods*. Department of Mechanical Engineering, Technical University of Denmark.

DNVGL-RP-C203 (2016, April). *Fatigue design of offshore steel structures*. DNVGL.

DNVGL-RP-C210 (2019, January). *Probabilistic methods for planning of inspection for fatigue cracks in offshore structures*. DNVGL.

DNVGL-ST-0126 (2018, July). *Support structures for wind turbines*. DNVGL.

Faber, M. H. (2000, April). Reliability based assessment of existing structures. *Progress in Structural Engineering and Materials 2*, 247–253.

Igwemezie, V., A. Mehmanparast, & A. Kolios (2018). Materials selection for xl wind turbine support structures: A corrosion-fatigue perspective. *Marine Structures 61*, 381 – 397.

JCSS (2011, April). *JCSS probabilistic model code, Part 3: Resistance models*. JCSS.

Mai, Q., J. Sørensen, & P. Rigo (2016, June). Updating failure probability of a welded joint in offshore wind turbine substructures. In *Proceedings of The 35th International Conference on Ocean, Offshore and Arctic Engineering Conference (OMAE16)*.

Newman, J. & I. Raju (1981). An empirical stress-intensity factor equation for the surface crack. *Engineering Fracture Mechanics 15*(1), 185 – 192.

Radu, D. & A. Sedmak (2016, December). Welding joints failure assessment – fracture mechanics approach. *Bulletin of the Transilvania University of Brasov 9*(58), 119–126.

Straub, D. (2004). *Generic approaches to risk based inspection planning for steel structures*. Ph. D. thesis, Swiss Federal Institute of Technology, Zurich.